Received May 16, 2019, accepted June 13, 2019, date of publication July 16, 2019, date of current version October 4, 2019.

Digital Object Identifier 10.1109/ACCESS.2019.2929361

Dynamic Analysis and Improvement of the Electrohydraulic System Under Power Limitation Control

SHAQI LUO[1], MIN CHENG[1], BING XU[2], RUQI DING[3], AND ZENAN HAN[1]
[1]State Key Laboratory of Mechanical Transmissions, Chongqing University, Chongqing 400044, China
[2]State Key Laboratory of Fluid Power and Mechatronic Systems, Zhejiang University, Hangzhou 310027, China
[3]School of Mechatronic Engineering, East China Jiaotong University, Nanchang 330029, China

Corresponding author: Min Cheng (chengmin@cqu.edu.cn)

This work was supported in part by the National Natural Science Foundation of China under Grant 51605050, Grant 91748210, and Grant U1509204, and in part by the Chongqing Research Program of Basic Research and Frontier Technology under Grant cstc2016jcyjA0253.

ABSTRACT With the electronization process of mobile hydraulics moving forward, the basic demand of power limitation control is increasingly fulfilled by electronic pump controllers to replace hydro-mechanical regulators. However, the nonlinear power controller introduces additional dynamics and potential oscillations into the electrohydraulic system. In this paper, the dynamic performance of the electrohydraulic system is analyzed using the linearized mathematical model and root locus tool, considering the factors of pump dynamic, actuator dimension, power setting point, and so on. A pump-based virtual leakage compensator is designed to reduce oscillations due to low damping excited by the power controller. The stability and parameter selection are then discussed to obtain optimal dynamic behavior. Using the traditional power controller as a comparison, the boom lifting motion test of a 2-ton excavator was carried out to validate the proposed compensator. The test result indicates that the proposed controller with optimized parameters has the ability to suppress pressure fluctuations and velocity oscillations.

INDEX TERMS Hydraulic control, power limitation, root locus, dynamic compensation, velocity oscillation.

I. INTRODUCTION

As one of the most important transmissions in mobile machinery, the advantages of hydraulic system are not only the high power-to-weight ratio [1], [2], but also the convenience of integrating multiple control functions, i.e. load-sensing [3], power limitation, and pressure protection. Traditionally, these functions are integrated into the hydro-mechanical pump by installing hydraulic valves and regulating mechanisms, e. g., constant power regulators used to avoid engine stall [4], [5]. The electrohydraulic technology, distinguished from traditional hydro-mechanical systems, is featured by the advantages of higher flexibility and better adaptation. The basic flow and power functions of the electrohydraulic pump are achieved by developing multi-purpose electronic controllers. For instance, Hansen and his colleagues presented an electronic load sensing system [6], [7], in which the system mechanical complexity was reduced by transferring features as flow-sharing, power-sharing and high pressure protection to electronic control. Ruggeri et al. developed an embedded electronic control unit to implement additional controls on the pump, e.g., torque, power, anti-stall and variable load sensing [8]. Also, several related patents have been authorized [9], [10], and commercial products of multi-function electrohydraulic pumps have entered into the market already [11], [12].

This paper discusses on electronic control of power limitation. From the aforementioned literatures, the function of electronic power limitation is achieved usually by regulating the pump displacement so that the product of theoretical pump flow and pump pressure equals to the setting power value [6]. Thus, the pump control signal is limited as $u_p = P_n/k_{pp}p_pn_p$. Previous works are focused on improving the dynamic performance of the pump itself. Khalil *et al.* proposed a single feedback control loop to suppress the steady state vibration of the swash plate [13]. Anis *et al.* designed a fuzzy logic controller to decrease the settling time of the pump [14]. However, from the view of control, the power limitation controller is a highly nonlinear one, which introduces additional dynamic behavior especially with relatively

The associate editor coordinating the review of this manuscript and approving it for publication was Taufik Abrao.

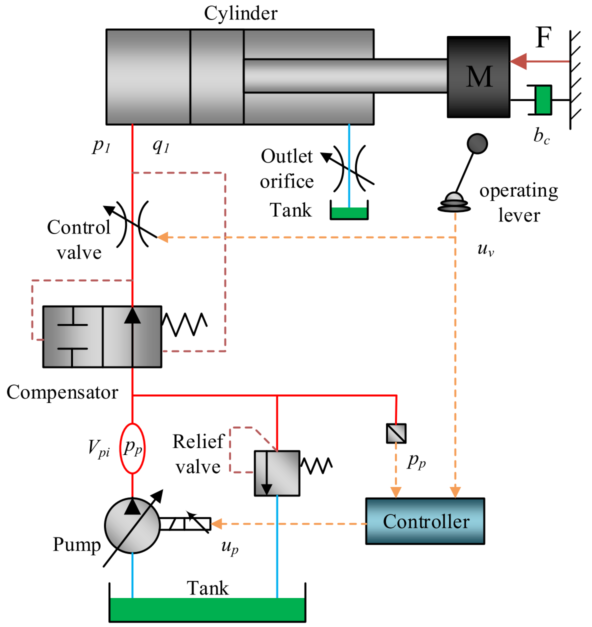

FIGURE 1. Scheme of the pump-based constant-power control system.

slow pump response. The system stability and the dynamic performance are doubtful and rarely discussed in the existing literatures. The cylinder load or velocity is relatively high when power limitation is active. Thus, the oscillation or instability issue of the system under power limitation should be an important concern, considering machine safety and operation of comfort.

In this paper, the stability and dynamic performance are analyzed by the linearized mathematical model, considering the factors of pump dynamic, pressure variation, power setting point and so on. Moreover, a pump-based virtual leakage compensation method is proposed via pressure feedback to dampen and improve the system behavior. The rest of paper is divided into five sections. Firstly, in Section II, the mathematical model of the studied system is established. The dynamic analysis and the controller design are given in Section III and Section IV, respectively. Then, the test rig and experiment results are shown in Section V. Last, in Section VI, the conclusion is drawn.

II. SYSTEM MODEL

A. MATHEMATICAL MODELING

Illustrated in Fig. 1, the electrohydraulic control system consists of an electrically controlled pump, a relief valve, a primary pressure compensator, a proportional directional valve (PDV) acting as the control valve, a cylinder and so on. The controller receives pump pressure signal p_p and the input signal of PDV u_v from operating lever. Then, based on pressure feedback signals, the controller provides control signal to the electrically controlled pump, which is driven by a motor.

The main function of the constant-power controller usually consists of two parts: a load sensing part and a power limitation one. It complicates the hydraulic circuit and impairs flexible control in mobile machinery. As for the velocity control, the primary pressure compensator and two pressure transmitters are employed in the system as depicted in Fig. 1, in order to track the reference velocity on the base of differential pressure of PDV. In fact, there are different approaches to get cylinder velocity, such as velocity or flow sensors, which detect directly or indirectly. However, as so far, in mobile machineries, they are too sensitive or expensive to adopt [16]. Therefore, pressure sensor is a preferable choose in practical applications. Another advantage of pressure transmitters is that the output power of the pump can be calculated online via multiplying the pressure by the pump flow rate.

In the studied system, the pump linked with a motor rotates at a fixed speed. The dynamic of the pump displacement can be modeled as a first-order system by the transfer function [17]:

$$V_p = \frac{\omega_p}{s+\omega_p} k_{pp} u_p\left(s\right) \tag{1}$$

Considering the pump leakage, the supplied flow of the pump can be expressed as follow:

$$q_p(s) = n_p \cdot V_p(s) - k_{lp} \cdot p_p(s) \tag{2}$$

The continuity equation for the chamber between the pump and the control valve can be expressed by Eq. (3), at times of the fully closed relief valve.

$$p_p\left(s\right) = \frac{\beta_e}{V_{pi} s}\left[q_p\left(s\right) - q_1\left(s\right)\right] \tag{3}$$

In a pressure compensated system armed with only one single actuator, the pressure compensator is fully opened. Therefore, in this situation, for simplifying the modeling process, the pressure loss of the compensator and the oil flowing into its pilot chamber are ignored. Hence, under a curtain working condition, the linearized expression for the flow rate of the valve can be described as:

$$q_1\left(s\right) = k_q x_v\left(s\right) + k_{pq}\left[p_p\left(s\right) - p_1\left(s\right)\right] \tag{4}$$

The continuity equation in the meter-in chamber is described as:

$$p_1\left(s\right) = \frac{\beta_e}{V_1 s}\left[q_1\left(s\right) - A_1 v_c\left(s\right)\right] \tag{5}$$

As depicted in Fig. 1, the cylinder leakage is elided, since it contributes to damping. The pressure drop across the outlet orifice is also neglected during the modeling process, because the load is usually quite heavy when constant-power function is triggered. Accordingly, the piston motion equation can be described as follow:

$$\left(M_e s + b_c\right) v_c\left(s\right) = A_1 p_1\left(s\right) - F_e\left(s\right) \tag{6}$$

Since the differential pressure of every PDV is limited by the pressure compensator, respectively, the supplied flow rate can be written as follow:

$$q_{vi} = C_d A\left(x_{vi}\right)\sqrt{\frac{2\Delta p_{nom}}{\rho}}, \quad i = 1, 2, \ldots, n \tag{7}$$

According to the working principle of the constant power function [7], the control signal of pump can be expressed as:

$$u_{po}(t) = \begin{cases} \dfrac{q_{max}}{n_p k_{pp}}, & 0 \le p_p(t) \le \dfrac{P_n}{q_{max}} \\ \dfrac{P_n}{p_p(t)\, n_p k_{pp}}, & \dfrac{P_n}{q_{max}} < p_p(t) < p_{max} \\ \dfrac{P_n}{p_{max} n_p k_{pp}}, & p_p(t) \ge p_{max} \end{cases} \tag{8}$$

When the power is lower than preset P_n, the controller works in the load sensing mode, whose output signal is assumed as $u_{pe}(t)$. And it will work as a constant-power valve/controller, if the system consumption is higher than P_n. The control signals are therefore the smaller value of the signal in the two controllers, see Eq. (9).

$$u_p(t) = min\left[u_{po}(t), u_{pe}(t)\right] \tag{9}$$

In practical applications, the system parameters can be adjusted online. Therefore, it provides a convenient approach to change the constant-power point P_n for adapting to different specific working conditions, which contributes to flexible control ability.

The pump leakage and the load viscousness contribute to damping improvement, so neglecting their effects helps to achieve the intended goal. From Eqs. (1)-(8), the transfer function of the cylinder velocity can be deduced and expressed as follow:

$$v_c(s) = \frac{N_1 u_p(s) - N_2 F_e(s)}{K_4 s^4 + K_3 s^3 + K_2 s^2 + K_1 s + K_0} \tag{10}$$

where

$$\begin{aligned} N_1 &= A_1 \beta_e (V_{pi} s^2 + \omega_p V_{pi} s + \omega_p P_n \beta_e / p_{p0}^2) \\ N_2 &= V_1 V_{pi} s^3 + \beta_e k_{pq} (V_1 + V_{pi}) s^2 + \omega_p \beta_e (k_{pq} (V_{pi} + V_1) \\ &\quad + P_n / p_{p0}^2) s + \omega_p \beta_e k_{pq} P_n / p_{p0}^2 \\ K_4 &= M_e V_1 V_{pi} \\ K_3 &= M_e \beta_e k_{pq} (V_{pi} + V_1) + \omega_p M_e V_1 V_{pi} \\ K_2 &= \omega_p M_e \beta_e (k_{pq} V_{pi} + k_{pq} V_1 + V_1 P_n / p_{p0}^2) + \beta_e A_1^2 V_{pi} \\ K_1 &= A_1^2 \beta_e^2 k_{pq} + \omega_p M_e P_n / p_{p0}^2 + \omega_p A_1^2 \beta_e V_{pi} \\ K_0 &= \omega_p A_1^2 \beta_e^2 (P_n / p_{p0}^2 + k_{pq}) \end{aligned}$$

III. DYNAMIC ANALYSIS

In the studied system, there are lots of parameters which have influences on pole locations and the system dynamic performance. Some of them are unalterable but others can be adjusted.

The pump natural frequency ω_p and the rodless cavity area A_1, are unchangeable in most mobile machinery, but it is important to know how they affect the damping. For example, analyzing effects caused by ω_p helps to know whether a lower ω_p can be an obstacle to get an appropriate damping ratio. The constant-power point P_n and the pump pressure p_{p0} are changeable and also crucial for improving the damping ratio.

Accordingly, the root locus [15] with respect to four typical parameters will be calculated and analyzed, respectively.

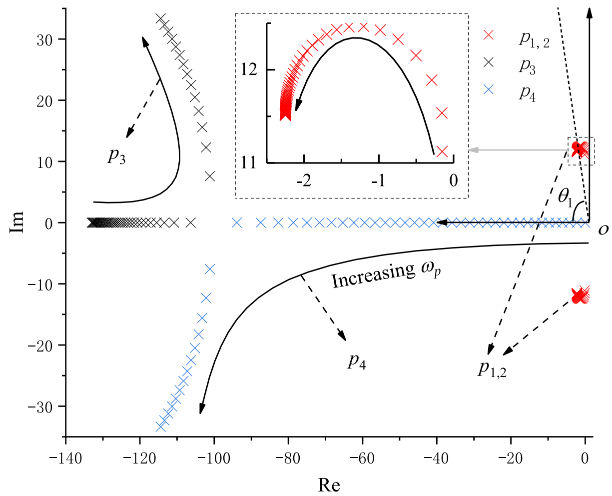

FIGURE 2. Pole locations with respect to pump natural frequency ω_p.

TABLE 1. Parameters used to determine the pole locations.

Parameters	Value	Parameters	Value
A_1 (m^2)	0.0038	k_{cp} (V/MPa)	0.48951
k_{pp} [m^3/(rad·V)]	7.26×10^{-7}	k_q [m^3/(s·V)]	0.0001
k_{pq} [m^3/(s·Pa)]	1×10^{-10}	P_n (kW)	1.2
p_{p0} (MPa)	8	V_1 (m^3)	0.003
V_{pi} (m^3)	0.001	M_e (Kg)	3×10^4
ω_p (rad/s)	45.84	ω_{cp} (rad/s)	7.5746
β_e (MPa)	1000	n_p (rev/min)	1500

A. PUMP NATURAL FREQUENCY ω_p

Generally, the dynamic performance is determined by the locations of poles and zeros. Therefore, the pole locations as a function of ω_p are shown in Fig. 2 by Eq. (10) with parameters in Table 1. In order to illustrate how the pole locations change as the pump natural frequency ω_p varies, ω_p is assumed to increase from 0.01 to 100 rad/s. As depicted in Fig. 2, the four poles are all located on the left half-plane, which are expressed as follow:

$$p_{1,2} = -a \pm bj \tag{11}$$

$$\begin{cases} p_3 = -c \\ p_4 = -d \end{cases} or \begin{cases} p_3 = -c + ej \\ p_4 = -c - ej \end{cases} \tag{12}$$

where $a, b, c, d, e > 0$.

It can be inferred that p_3 does not exert a great influence on the dynamic performance, since c/a is much larger than l, whose value range is between 3 and 5, when ω_p increases from 0.01 to 100 rad/s. Similar to the p_3 case, the location of p_4 dose not need to be considered if ω_p exceeds a certain value. However, when ω_p is smaller than the threshold value, it is not obvious that which one, p_4 or $p_{1,2}$, determines the dynamic performance. One potential drawback is that a small ω_p contributes to lower damping, since the angle θ between conjugate pole and negative real axis (take θ_1 showed in Fig. 2 for example) becomes extremely large when ω_p increases,

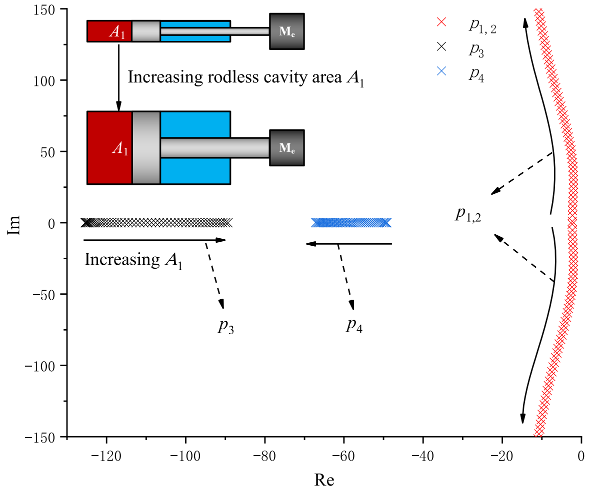

FIGURE 3. Pole locations with respect of rodless cavity area A_1.

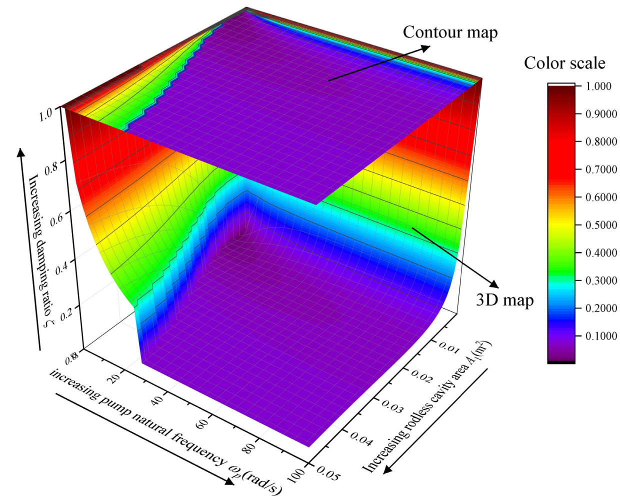

FIGURE 4. Damping with respect to the pump natural frequency ω_p and rodless cavity area A_1.

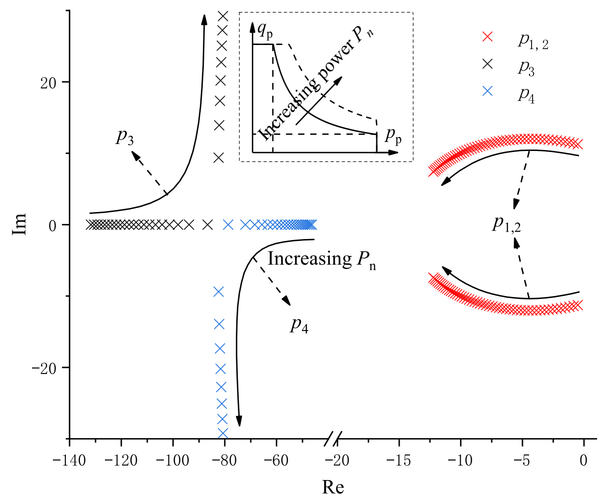

FIGURE 5. Pole locations with respect to constant-power point P_n.

and $\zeta_{1,2}$ can be calculated by $\theta_{1,2}$, see Eq. (13). Moreover, another disadvantage is that the system stability becomes poor, for the reason that p_4 is located near the imaginary axis which contributes to lower stability margin.

$$\theta_{1,2} = \arccos \zeta_{1,2} = \arctan \frac{\sqrt{1-\zeta_{1,2}^2}}{\zeta_{1,2}}$$
$$\Rightarrow \zeta_{1,2} = \frac{a}{\sqrt{a^2+b^2}} \tag{13}$$

B. RODLESS CAVITY AREA A_1

Depended on the default parameters in Table 1, the pole locations with respect to the rodless cavity area A_1 (from 0.0008 to 0.05 m^2) can be obtained and illustrated in Fig. 3. Similar to ω_p case, p_3 and p_4 have little influence on pole locations because c/a and d/a are far more than l. Therefore, the dynamic performance is decided by the locations of $p_{1,2}$. According to Fig. 3 and Eq. (13), the damping ratio $\zeta_{1,2}$ derived from $p_{1,2}$ is positively correlated with A_1. Therefore, the conclusion can be drawn that the increase of rodless cavity area A_1 contributes to higher damping ratio.

1) DAMPING WITH RESPECT TO ω_p AND A_1

In Fig. 4, the damping ratio as a function of ω_p and A_1 is presented in two ways: contour map and 3D map. It can be concluded that the increase of A_1 contributes to damping improvement, when ω_p is less than a certain value. However, the contribution will be dramatically impaired if ω_p exceeds the threshold value. As for ω_p, its influence on damping ratio is similar to A_1 case. The damping ratio is positively correlated with ω_p only when A_1 is relatively small. Therefore, the effects derived from alterations of ω_p and A_1 can be concluded as follows:

i) Only when ω_p (or A_1) is in an appropriate range, can a higher A_1 (or ω_p) provide better damping performance.

ii) If the values of ω_p and A_1 are extremely small or greater than the threshold value, the system will be in a low damping situation.

C. CONSTANT-POWER POINT P_N

The pole locations pertaining to the constant-power point P_n is exhibited in Fig. 5. Since c/a and d/a are both larger than l, $p_{1,2}$ can be guaranteed to be the dominated poles, which determine the dynamic performance of the system. By analyzing the $\zeta_{1,2}$ derived from $p_{1,2}$ and Eq. (13), it can be concluded that the damping performance will be better, gradually, with the increase of P_n.

D. PUMP PRESSURE P_{P0}

In Fig. 6, the pole locations as a function of the pump pressure p_{p0} is shown. Similar to the former case, $p_{1,2}$ can dominate the dynamic performance, while p_{p0} alters from 4MPa to 22MPa. It means that the contribution from $p_{3,4}$ can totally be discarded. And there is a negative relationship between p_{p0}

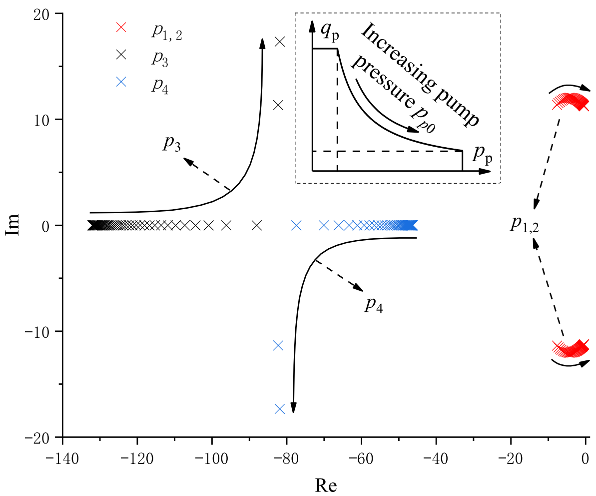

FIGURE 6. Pole locations with respect to pump pressure p_{p0}.

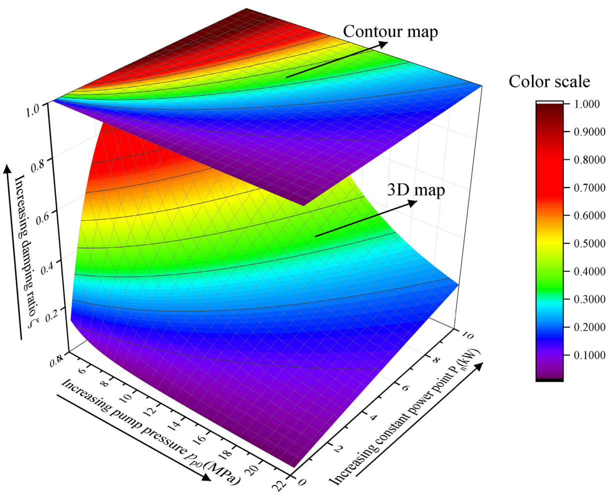

FIGURE 7. Damping with respect to constant-power point P_n and the pump pressure p_{p0}.

and damping ratio, which means a lower pump pressure in the allowed range can result in better damping performance.

1) DAMPING WITH RESPECT TO P_N AND P_{P0}

Illustrated in Fig. 7, the damping as a function of P_n and p_{p0} is shown in two different ways: contour map and 3D map. By observing Fig. 7, the conclusion can be drawn that a higher P_n or a lower p_{p0} in the allowed range can provide better damping performance.

IV. CONTROL DESIGN

As for the control, the vibration suppression is an important field attracted to lots of researchers. Therefore, methods to resolve it have emerged in large numbers, and can be divided into two categories: 1) pure hydraulic approach and 2) electrohydraulic approach. The former usually employs a bypass valve and an accumulator to damp vibration, which causes other problems such as bypass leakage and more time to build up the pressure, and also with the common disadvantages of poor flexibility like the traditional hydraulic system. The later usually detects the oscillation first and then damps it via adjusting the valve or pump. Lots of physical signal e.g. displacement or acceleration can be detected and processed. However, compared with the other signal, dynamic pressure feedback (DPF) is reliably and flexibly available on mobile machineries and also has been employed in practical applications and academic researches [18]–[22]. Accordingly, aiming at the vibration suppression, a control approach based on the DPF and its analyses are carried out in this section.

A. CONSTANT-POWER CONTROL WITH VIRTUAL LEAKAGE COMPENSATION (CPVC)

In Section III, it can be concluded that higher pump pressure p_{p0}, lower constant-power point P_n, or an inappropriate pump natural frequency ω_p and rodless cavity area A_1 can produce side-effects in the damping performance and system stability. Although they can be optimized before manufacture, they are unalterable in most practical applications. A popular approach to optimize the damping is to modify the shape or area of meter-out orifice [16]. However, the drawback is that it is difficult to make a trade-off between fast response and high stability. Besides, the unchangeable orifice shape can not adapt to the load variation in most applications [23].

In order to find an approach to solve the mentioned problem, the real-time pump pressure signal is used to suppress the system vibration. The modified control signal consists of u_{po} mentioned in Eq. (8) and a compensation signal derived from the pump pressure. Accordingly, the virtual compensation signal, at times of constant-power mode, is expressed as:

$$u'_{po}(s) = u_{po}(s) - \frac{k_{cp}s}{s+\omega_{cp}}p_p(s) \tag{14}$$

$$u'_p(t) = min\left[u'_{po}(t), u_{pe}(t)\right] \tag{15}$$

In order to analyze in the complex frequency domain, when $P_n/q_{max} < p_p(t) < p_{max}$ and the pump pressure is assumed as p_{p0}, the control signal of pump can be therefore linearized and expressed as follow:

$$\Delta u_{po}(t) = -\frac{P_n}{n_p k_{pp} p_{p0}^2}\Delta p_p(t) \tag{16}$$

Working in constant-power mode, the pump flow rate can be inferred from Eqs. (2) and (8), see Eqs. (17) and (18).

$$q_p(s) = \left(\frac{n_p k_{pp}\omega_p}{s+\omega_p}\cdot\frac{P_n}{p_{p0}^2} - k'_{lp}(s)\right)p_p(s) \tag{17}$$

$$\begin{aligned} k'_{lp}(s) &= k_{lp} + \frac{n_p k_{pp}\omega_p}{s+\omega_p}\cdot\frac{k_{cp}s}{s+\omega_{cp}} \\ &= k_{lp} + \frac{k_{bp}\zeta\omega_0 s}{s^2+\zeta\omega_0 s+\omega_0^2} \end{aligned} \tag{18}$$

where

$$k_{bp} = \frac{n_p k_{pp} k_{cp}\omega_p}{\omega_p+\omega_{cp}}, \zeta = \frac{\omega_p+\omega_{cp}}{\sqrt{\omega_p\omega_{cp}}},$$
$$\omega_0 = \sqrt{\omega_p\omega_{cp}}$$

From Eq. (17), it can be known that the k'_{lp} consists of two parts: one is the constant value k_{lp} and the other is a second-order band-pass filter. Accordingly, when the vibration frequency is between $f_1 = \omega_{cp}/2\pi$ and $f_2 = \omega_p/2\pi$, k'_{lp} will be far larger than k_{lp}. The controller seems to increase the pump leakage, during the vibration. Considering this effect, the method is called virtual leakage compensation in the after text. Higher pump leakage can provide better damping performance. Moreover, k'_{lp} is equal to k_{lp} at times of steady-state conditions, owing to the function of band-pass filter. Thus, k'_{lp} does not affect the steady-state speed of the cylinder. All those mentioned characteristics indicate that k'_{lp} gives an adaptive virtual leakage to the pump. It means that the pump has the ability to provide a higher damping ratio only when vibrations occur.

The expression of actuator velocity under power limitation can be drawn from Eqs. (10) and (14), see Eq. (19).

$$v_c(s) = \frac{N'_1 u_p(s) - N'_2 F_e(s)}{K'_5 s^5 + K'_4 s^4 + K'_3 s^3 + K'_2 s^2 + K'_1 s} \tag{19}$$

where

$$\begin{aligned}
N'_1 &= A_1 \beta_e k_q \Big[V_{pi} s^3 + V_{pi}(\omega_p + \omega_{cp}) s^2 + \big(V_{pi}\omega_p\omega_{cp} \\
&\quad + V_{pi}\omega_p\omega_{cp} + \beta_e\omega_p P_n/p_{p0}^2 + \beta_e \omega_p n_p k_{pp} k_{cp} \big) s \\
&\quad + \beta_e \omega_p \omega_{cp} P_n / p_{p0}^2 \Big] \\
N'_2 &= N_2 \left[s^2 + (\omega_p + \omega_{cp}) s + \omega_p\omega_{cp} \right] \\
K'_5 &= M_e V_{pi} V_1 \\
K'_4 &= M_e V_{pi} V_1 (\omega_p + \omega_{cp}) + M_e \beta_e k_{pq} (V_{pi} + V_1) \\
K'_3 &= M_e V_{pi} V_1 \omega_p \omega_{cp} + M_e \beta_e k_{pq} (V_{pi} + V_1)(\omega_p + \omega_{cp}) \\
&\quad + M_e \beta_e V_1 \left(\omega_p P_n/p_{p0}^2 + \omega_p n_p k_{pp} k_{cp} \right) + A_1^2 \beta_e V_{pi} \\
K'_2 &= M_e \beta_e k_{pq} (V_{pi} + V_1) \omega_p \omega_{cp} + M_e \beta_e V \omega_p \omega_{cp} P_n / p_{p0}^2 \\
&\quad + M_e k_{pq} \beta_e^2 \left(\omega_p P_n/p_{p0}^2 + \omega_p n_p k_{pp} k_{cp} \right) + A_1^2 \beta_e^2 k_{pq} \\
&\quad + A_1^2 \beta_e V_{pi} (\omega_p + \omega_{cp}) \\
K'_1 &= A_1^2 \beta_e^2 \left[\omega_p P_n/p_{p0}^2 + \omega_p n_p k_{pp} k_{cp} + k_{pq}(\omega_p + \omega_{cp}) \right] \\
&\quad + A_1^2 \beta_e V_{pi} \omega_p \omega_{cp} + M_e k_{pq} \beta_e^2 \omega_p \omega_{cp} P_n / p_{p0}^2 \\
K'_0 &= A_1^2 \beta_e^2 \left(\omega_p \omega_{cp} P_n / p_{p0}^2 + k_{pq} \omega_p \omega_{cp} \right)
\end{aligned}$$

B. STABILITY ANALYSIS

The Eq. (19) is a fifth-order system, whose stability condition can be therefore inferred from the Routh-Hurwitz criteria:

$$\begin{cases}
K'_5 > 0 \\
K'_4 > 0 \\
K'_3 - K'_2 K'_5 / K'_4 > 0 \\
K'_2 - (K'_4 K'_1 - K'_0 K'_5) / (K'_3 - K'_2 K'_5 / K'_4) > 0 \\
K'_1 - (K'_0 K'_3 - K'_0 K'_2 K'_5 / K'_4) / (K'_2 - (K'_4 K'_1 \\
\quad + K'_0 K'_5) / (K'_3 - K'_2 K'_5 / K'_4)) - K'_0 K'_5 / K'_4 > 0 \\
K'_0 > 0
\end{cases} \tag{20}$$

From Eq. (20), it is easy to know that K'_5, K'_4, K'_0>0 can be satisfied no matter how parameters alter, but it is very troublesome to confirm those rest criteria in Eq. (20). It should be mentioned that the build-in solver '*fimincon*' in MATLAB [24] can figure out almost the minimum value when parameters alter in a given range. By this means, the studied system can be confirmed and guaranteed to satisfy the rest three criteria in Eq. (20) with parameters in Table 1.

C. CONTROL PARAMETERS

Since most structural parameters are not easy to alter in mobile machinery, the key factor of damping improvement is therefore to adjust the following parameters:

1) LOWER CUT-OFF ANGULAR FREQUENCY ω_{cp}

The ω_{cp} should be below the vibration angular frequency ω_h of the studied system [25], and also smaller than the upper cut-off angular frequency ω_p. Since the cylinder back pressure is almost equal to the drain line pressure, whose contribution to the vibration frequency can be elided. Therefore, ω_{cp} can be estimated by Eq. (21).

$$\omega_{cp} < \omega_h = \sqrt{\frac{\beta_e A_1^2}{M_e V_1}} < \omega_p \tag{21}$$

In Fig. 8, the pole locations as a function of ω_{cp} are shown, while ω_{cp} increases from 0.01 to ω_p with parameters in Table 1. Compared with the pole locations of original system (marked as "without CPVC"), it is easy to know that no matter how ω_{cp} alters in the given range, higher damping can be obtained via observing θ. When ω_{cp} is below a threshold, the added p_5 dominates system dynamic, which means the studied system can be almost described by a first-order system. Although a first-order system means high damping, the system stability may even become poor since p_5 locates near the imaginary axis, which makes system stability margin excessively low. If ω_{cp} is larger than the certain value, the system can be described by a second-order system, and the damping will get lower when ω_{cp} continues to increase. Therefore, the optimization will always be a compromise between high damping and good stability margin.

2) THE GAIN OF VIRTUAL LEAKAGE COMPENSATION K_{cp}

k_{cp} with respect to the pole locations is depicted in Fig. 9, when k_{cp} alters from 0.0001 to 1 with parameters in Table 1. By observing θ of $p_{1,2}$, it is known that k_{cp} is positively correlated with the damping, although p_5 may exert an influence, when k_{cp} is relatively high. However, at times of increasing damping, another problem of phase-lag appears, owing to the increase of a.

In conclusion, an extremely low or high ω_{cp} contributes to lower stability margin and lower damping, respectively. As for k_{cp}, an immoderately low value contributes almost nothing to damping, and an excessively high value makes the phase-lag increase. Therefore, the optimum dynamic

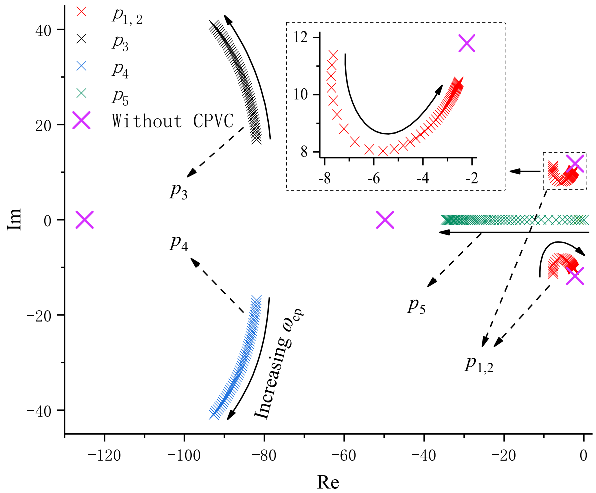

FIGURE 8. Pole locations with respect to ω_{cp}.

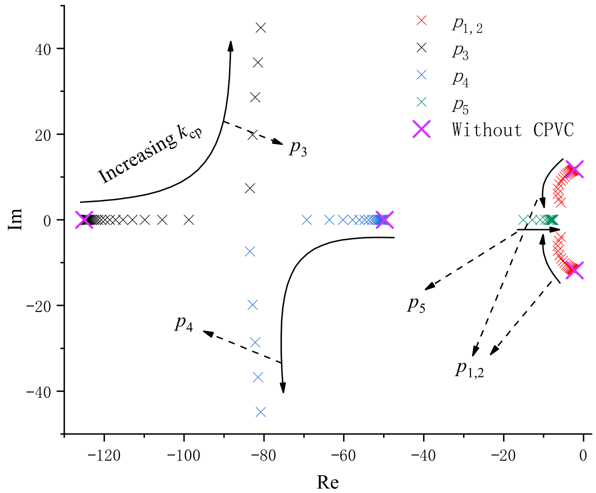

FIGURE 9. Pole locations with respect to k_{cp}.

performance is always a trade-off among system stability margin, damping ratio and phase-lag.

V. EXPERIMENTAL VERIFICATION

Depicted in Fig. 10, the development of proposed controller was based on xPC Target RTW (Real-time Workshop) with host and target computers. It was operated on the MATLAB/Simulink, which was very user friendly and supplied a way to acquire and process for real-time signals. The proposed controller was deployed on a 2-ton mini-excavator, by which experiments had been done to test and verify it. The experiments are divided into two parts:

A. Verification of CP and CPVC function;
B. Effect of different k_{cp} on system performance.

A. VERIFICATION OF CP AND CPVC FUNCTION

The boom lifting depicted in the 4th graph of Fig. 11 was regarded as a typical movement [16], which was executed in three different modes:

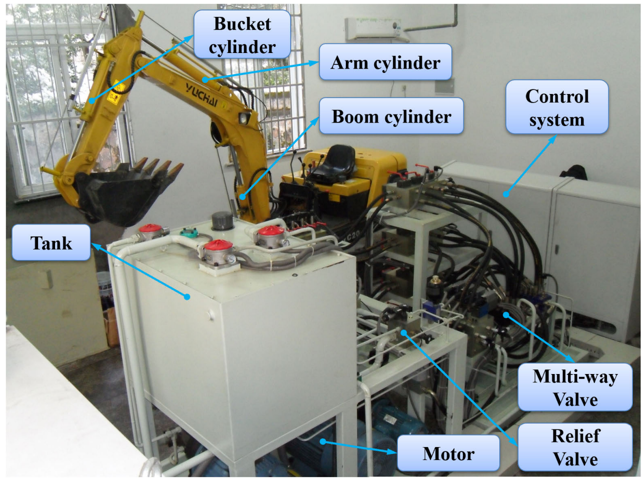

FIGURE 10. Photograph of the test rig.

TABLE 2. Parameters used in the test.

Parameters	Value	Parameters	Value
P_n (kW)	1.35	p_{max} (MPa)	12
k_{cp} (V/MPa)	0.3	ω_{cp} (rad/s)	0.5
n_p (rev/min)	1500	Max V_p (mL/r)	45.6

1) The mode without CPVC is marked as "no CPVC", which means that the controller runs without power limitation and virtual leakage compensation;
2) The mode marked as "only CP" is armed with power limitation but without virtual leakage compensation, in order to verify the function expressed as Eq. (8);
3) The mode marked as "CPVC" is equipped with not only the function of constant-power but also virtual leakage compensation (expressed as Eq. (14)).

The input, who contains three step-function signals, from the operating lever to the control valve (depicted in Fig. 1) is shown in the 2nd graph of Fig. 11. Stimulated by those inputs, experimental results of boom cylinder contain the control signal, the cylinder velocity, the pump pressure and power consumption, which are all illustrated specifically in Fig. 11.

In order to describe more specifically, results can be divided into four segments by three step-function signals as shown at the top of Fig. 11.

1) *SEGMENT* I:

The control valve was held in the middle position, while its control signal was equal to 6 V. Accordingly, at times of this part, the pump signal from controller was about 0 V, in all modes. Therefore, cylinder velocity, pump pressure and power stayed the same.

2) *SEGMENT* II:

By observing the 1st picture of Fig. 11, those indexes themselves (such as the pump signal, the system power, etc.) do not exist apparent difference in different modes, during this whole segment. The reason is that the system power did not

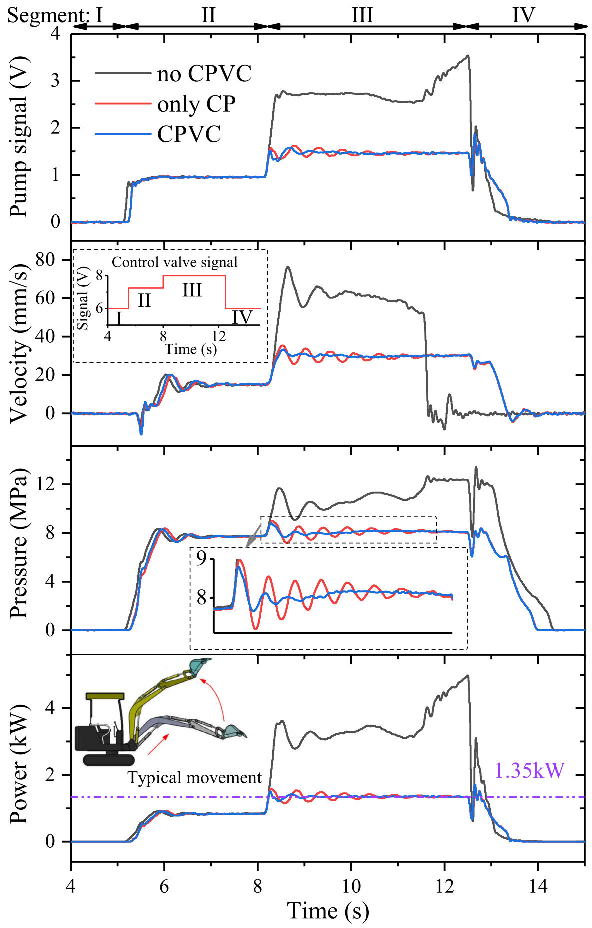

FIGURE 11. Experimental results of boom cylinder in three different modes.

reach the preset P_n, therefore, all controllers worked as ''load-sensing'' controller in order to supply demanded flow rate.

3) *SEGMENT* III:

In CP and CPVC modes, the controllers acted as ''constant-power'' controller, owing to system consumption beyond P_n. Therefore, all indexes, such as the system power, rose and then remained constant overall, despite fluctuation, when CP function is triggered. With regard to the fluctuation, in CP mode, the boom cylinder vibrated violently about 5 cycles before stabilizing within 5 %. However, the times of vibration decreased from 5 to 1 by adding virtual leakage compensation, in CPVC mode. By contrast, the system power and other indexes in no CPVC mode was much more than those in CP or CPVC mode. More specifically, the highest point of the power consumption, in no CPVC mode, was about 5 kW and far more than the preset P_n, since the controller in no CPVC mode worked as a ''constant-flow'' controller with no power limitation, just in order to supply the demanded flow for the control valve. As for the error and accuracy, from 8.23 s (the first time of reaching at 1.35 kW) to 12.00 s, the RMSEs (Root Mean Squared Error) of the system power in CP and CPVC modes are 0.0845 kW and 0.033 kW, respectively.

TABLE 3. In *Segment* III, dynamic performance specifications of the cylinder velocity in three different modes.

	no CPVC	only CP	CPVC
Rise time (s)	0.190	**0.120**	0.150
Settling time (s)	———	3.200	**1.409**
Overshoot (%)	27.951	20.001	**14.029**
Peak (mm/s)	76.348	35.386	**33.432**
Peak time (s)	0.640	**0.530**	0.540

Moreover, the control precisions in the two modes are 6.26% and 2.44%, respectively. Therefore, it can be drawn that adding virtual leakage compensation can also contribute to improve the control precision.

Besides, more specifications about dynamic performance of the cylinder velocity in three different modes are listed in Table 3. The settling and peak time are counted from the eighth second. From the perspective of the cylinder velocity, CPVC mode is obviously better than other two modes in the aspect of indicator settling time, overshoot and peak.

4) *SEGMENT* IV:

All indexes, in all modes, gradually reduced to 0 during this segment, and there was no apparent difference among all indexes in CP and CPVC modes. However, in no CPVC mode, the piston reached the end of cylinder stroke and its velocity had diminished to 0 at the end of previous segment, owing to its higher velocity in segment III.

B. EFFECTS OF DIFFERENT K_{CP} on system performance

Experimental results of boom cylinder in CPVC mode with different k_{cp} are illustrated in Fig. 12. A step signal for the control valve leaded to drastic changes in pump signal, which caused alterations in other indexes. Overall, all indexes stabilized at different constants, although there were some fluctuations and errors. To be more specifically, the experimental results are analyzed in four parts:

1) $K_{CP} = 0$

It can be known that all indexes vibrated several times before stabilization, when $k_{cp} = 0$ (only CP function without virtual leakage compensation), which met the results mentioned in Section V.A.

2) $K_{CP} = 0.1$

Vibrations of all indexes were suppressed, though not very obvious.

3) $K_{CP} = 0.3$

Compared with lower k_{cp}, fluctuations of the cylinder velocity are evidently suppressed, although there was a slight delay. Fortunately, the delay was so small that it could be ignored. It should be mentioned that the system power overshoot was lower than that of other parameters, but it was

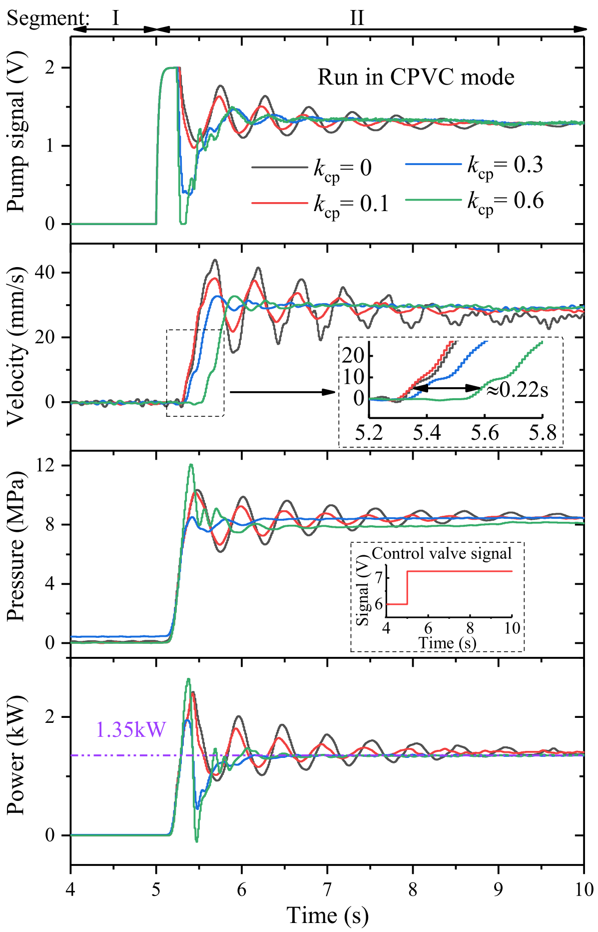

FIGURE 12. Experimental results of boom cylinder with different k_{cp} in CPVC mode.

followed by a lower trough. It seems like the P (Proportion) is slightly too large in a PID (Proportion, Integral, Differential) controller.

4) $K_{CP} = 0.6$

By observing the cylinder velocity, similar to $k_{cp} = 0.3$, vibrations were significantly suppressed too, but it should be mentioned that the delay cannot be neglected, since it was getting much larger than before (about 0.22s). Owing to the delay, while $k_{cp} = 0.6$, the piston position and load at the same time were quite different from them in lower k_{cp}, which leaded to a lower pump pressure than others when it was stable. As for the pump signal, the pump pressure and power, excessive k_{cp} provided larger amplitude in the first time of vibration, although it attenuated rapidly.

More specifications about dynamic performance of the cylinder velocity in three different modes can be found in Table 4. The settling and peak time are counted from the fifth second. Overall, $k_{cp} = 0.3$ provides a better dynamic performance via observing settling time, overshoot (almost smallest) and peak.

In general, all those experimental results agreed with the conclusion in Section IV.

TABLE 4. In *Segment* II, dynamic performance specifications of the cylinder velocity in CPVC mode with different k_{cp}.

	k_{cp}=0	k_{cp}=0.1	k_{cp}=0.3	k_{cp}=0.6
Rise time (s)	**0.150**	**0.150**	0.230	0.230
Settling time (s)	4.959	3.889	**1.109**	1.309
Overshoot (%)	60.517	33.227	**11.315**	**11.148**
Peak (mm/s)	43.983	38.270	**32.729**	**32.729**
Peak time (s)	**0.679**	**0.679**	0.710	0.910

VI. CONCLUSION

Electronic pump controllers increasingly replace hydro-mechanical regulators to fulfill the basic demand: power limitation control, which is a highly nonlinear one and impairs the dynamic performance, such as system vibrations observed from actual test. In this paper, the dynamic performance is analyzed and improved for the electrohydraulic system under power limitation. The conclusion is summarized as follows:

1) Using the root locus method, it can be known that a higher rodless cavity area A_1 leads to a better damping performance only when the pump natural frequency ω_p is in an appropriate range. Similarly, a higher ω_p contributes to better damping performance if A_1 is in the appropriate range. If the values of ω_p and A_1 are extremely small or greater than the threshold value, stability margin will go down or system will be in a lower damping situation, respectively. Similar to A_1 and ω_p, only when constant power point P_n and the pump pressure p_{p0} are in the allowed range, a higher P_n or a lower p_{p0} can provide better damping performance.
2) In order to overcome disadvantages of poor flexibility and complex hydraulic circuit in traditional hydraulic system, a pump-based virtual leakage compensation controller under power-limitation is proposed. Experiments for validating proposed controller with optimized control parameters were done in a mini-excavator. Experiment results show that the designed controller can improve the dynamic performance under constant-power mode. The accuracy of power control is less than 5 %, at times of steady-state condition. The system vibration is effectively damped with optimized control parameters, which makes the designed controller have great application prospects in mobile machinery.

However, there are still some problems to overcome in the future. For example, because the upper cut-off frequency of band-pass filter is limited by the pump natural frequency, the controller may cannot meet the intended goal, in special working condition, and how to adjust parameters in real time is also a challenge. Even then, the proposed controller is promising in mobile machinery.

NOMENCLATURE

Symbol	Description
A_1	Capside area of the cylinder [m^2]
b_c	Load viscous damping [N·s/m]
C_d	Flow coefficient of the control valve
F_e	External force [N]
$f_{1,2}$	Lower, upper cut-off frequency of bandpass filter [rad/s]
k_{bp}	Gain of bandpass filter
k_{cp}	Gain of virtual leakage compensation [V/MPa]
k_{lp}	Pump leakage gain [m^3/(s·Pa)]
k'_{lp}	Pump virtual leakage gain [m^3/(s·Pa)]
k_{pp}	Pump gain [m^3/(rad·V)]
k_{pq}	Flow-pressure gain of the control valve [m^3/(s·Pa)]
k_q	Flow gain of the control valve [m^3/(s·V)]
M_e	Equivalent load mass [Kg]
n_p	Rotational speed of the motor [rev/min]
p_1	Capside pressure of the cylinder [Pa]
p_p	Pump pressure [Pa]
p_{p0}	Pump pressure at a working point [Pa]
p_{max}	Set pressure of the relief valve [Pa]
P_n	Constant power point [W]
q_1	Flow rate of meter-in orifice [m^3/s]
q_p	Supplied flow rate from the pump [m^3/s]
q_{vi}	Flow rate of the control valve [m^3/s]
q_{max}	Maximum supplied flow rate from the pump [m^3/s]
u_{pe}	Control signal derived from load-sensing function [V]
u_{po}	Control signal derived from constant-power function [V]
u'_{po}	Control signal based on constant-power function with virtual leakage compensation [V]
u_p	Control signal from proposed controller in CP m- ode [V]
u'_p	Control signal from proposed controller in CPVC mode [V]
V_p	Pump displacement [m^3]
V_{pi}	Chamber volume between the pump and the compensator [m^3]
V_1	Capside volume of the cylinder [m^3]
v_c	Cylinder velocity [m/s]
x_v	Opening of the control valve [m]
β_e	Effective bulk modulus [MPa]
Δp_{nom}	Differential pressure of the control valve [Pa]
ζ	Damping coefficient of bandpass filter
θ	Poles angle down from real axis [rad]
ρ	Oil density [Kg/m^3]
ω_0	Center frequency of bandpass filter [rad/s]
ω_{cp}	Cutoff frequency of virtual leakage compensation [rad/s]
ω_p	Natural frequency of the pump [rad/s]
ω_h	Angular frequency of the system vibration [rad/s]

REFERENCES

[1] W. Shen, H. Huang, Y. Pang, and X. Su, "Review of the energy saving hydraulic system based on common pressure rail," *IEEE Access*, vol. 5, pp. 655–669, 2017.

[2] R. Ding, J. Zhang, and B. Xu, "Advanced energy management of a novel independent metering meter-out control system: A case study of an excavator," *IEEE Access*, vol. 6, pp. 45782–45795, 2018.

[3] M. Ruggeri and M. Guidetti, "Variable load sensing and anti-stall electronic control with sliding mode and adaptne PID," in *Proc. JFPS Int. Symp. Fluid Power*, 2008, vol. 2008, nos. 2–7, pp. 301–306.

[4] O. Gad, M. G. Rabie, and R. M. EI-Taher, "Fiber-optic frequency shifter using a surface acoustic wave incident at an oblique angle," *J. Dyn. Syst. Meas. Control.*, vol. 124, no. 3, pp. 443–451, 2002.

[5] S. H. Park, J. M. Lee, and J. S. Kim, "Modeling and performance improvement of the constant power regulator systems in variable displacement axial piston pump," *Sci. World Journal.*, vol. 2013, Aug. 2013, Art. no. 738260.

[6] R. H. Hansen, "Advanced power management of a telehandler using electronic load sensing," in *Proc. 10th Int. Workshop Res. Educ. Mechatron.*, Glasgow, U.K., Sep. 2009, pp. 1–9.

[7] R. H. Hansen, T. O. Andersen, and H. C. Pedersen, "Development and implementation of an advanced power management algorithm for electronic load sensing on a telehandler," in *Proc. Bath/ASME Symp. Fluid Power Motion Control*, Bath, U.K., 2010, pp. 537–550.

[8] M. Ruggeri, M. Martelli, and E. Leati, "Variable load sensing electro-proportional valve with torque, power and anti-stall control for variable displacement axial piston pumps," in *Proc. 7th Int. Fluid Power Conf.*, Aachen, Germany, 2014.

[9] K. Ligenfelter and G. Lafayette, "Electronic torque and pressure control for load sensing pumps," U.S. Patent 15 120 900, Mar. 18, 2015.

[10] K. R. Lingenfelter, A. Bruns, C. Daley, V. Ewald, and D. Wakefield, "Electronic load sense control with electronic variable load sense relief, variable working margin, and electronic torque limiting," U.S. Patent 9 759 212 B2, Sep. 12, 2017.

[11] Industrial Products: Axial Piston Variable Pump A4VSO Series. Bosch Rexroth. Lohr am Main, Germany. [Online]. Available: https://md.boschrexroth.com/modules/BRMV2PDFDownload-internet.dll/re92050_2018-10.pdf?db=brmv2&lvid=1208146&mvid=13979&clid=20&sid=AB21AE92F45B5A9B289D282D9A48C990.borex-tc&sch=M&id=13979,20,1208146

[12] Industrial Products: K3VG Pump. Kawasaki. Japan. [Online]. Available: http://www.kpm-usa.com/wp-content/uploads/Axial-Piston-Pumps/K3VG/K3VG-P-1001-03-04.pdf

[13] M. K. B. Khalil, V. D. Yurkevich, J. Svoboda, and R. B. Bhat, "Implementation of single feedback control loop for constant power regulated swash plate axial piston pumps," *Int. J. Fluid power.*, vol. 3, no. 3, pp. 27–36, 2002.

[14] Y. H. Anis and S. A. Kassem, "Performance of constant power operated swash plate axial piston pumps with fuzzy logic controllers," in *Proc. ASME Int. Mech. Eng. Congr. Expo.* San Diego, CA, USA: Amer. Soc. Mech. Eng., Nov. 2013.

[15] H. M. Barra, K. E. L. Marcillo, E. M. Rocha, M. V. A. Nunes, R. B. de Araújo, and W. B. Junior, "A digital damping controller to increases the safety in hydraulic pumping systems," in *Proc. 13th IEEE Int. Conf. Ind. Appl. (INDUSCON)*, France, U.K., Nov. 2018, pp. 393–398.

[16] R. Ding, B. Xu, J. Zhang, and M. Cheng, "Self-tuning pressure-feedback control by pole placement for vibration reduction of excavator with independent metering fluid power system," *Mech. Syst. Signal Process.*, vol. 92, pp. 86–106, Aug. 2017.

[17] L. Wang, W. J. Book, and J. D. Huggins, "Application of singular perturbation theory to hydraulic pump controlled systems," *IEEE/ASME Trans. Mechatronics*, vol. 17, no. 2, pp. 251–259, Apr. 2012.

[18] C. Williamson, S. Lee, and M. Ivantysynova, "Active vibration damping for an off-road vehicle with displacement controlled actuators," *Int. J. Fluid Power.*, vol. 10, no. 3, pp. 5–16, 2009.

[19] C. C. DeBoer and B. Yao, "Velocity control of hydraulic cylinders with only pressure feedback," in *Proc. ASME Int. Mech. Eng. Congr. Expo.*, New York, NY, USA, 2001, pp. 1–9.

[20] D. Cristofori, A. Vacca, and K. Ariyur, "A novel pressure-feedback based adaptive control method to damp instabilities in hydraulic machines," *SAE Int. J. Commercial Vehicles*, vol. 5, no. 2, pp. 586–596, 2012.

[21] M. Cheng, B. Xu, J. Zhang, and R. Ding, "Pump-based compensation for dynamic improvement of the electrohydraulic flow matching system," *IEEE Trans. Ind. Electron.*, vol. 64, no. 4, pp. 2903–2913, Apr. 2017.

[22] S. Kukkonen and E. Mäkinen, "Performance of a pump controlled asymmetric actuator—A comparison of different control methods," in *Proc. SME/BATH Symp. Fluid Power Motion Control*, New York, NY, USA, 2014, pp. 1–10.

[23] D. B. Payne and J. R. Stern, "Design rules for high damping in mobile hydraulic systems," in *Proc. 13th Scand. Int. Conf. Fluid Power*, Linköping, Sweden, Jun. 2013, no. 92, pp. 13–20.

[24] *MATLAB User Manual Version R2016B*, MathWorks, Natick, MA, USA, 2016.

[25] E. Zæv, G. Rath, and H. Kargl, "Energy efficient active vibration damping," in *Proc. 13th Scand. Int. Conf. Fluid Power*, Linköping, Sweden, Jun. 2003, no. 92, pp. 355–364.

SHAQI LUO was born in Suining, China, in 1993. He received the B.Eng. degree in mechanical engineering from Chongqing University, Chongqing, China, in 2016, where he is currently pursuing the Ph.D. degree in mechanical engineering with the State Key Laboratory of Mechanical Transmission. His research interests include electrohydraulic control, hydraulic mechanical composite transmission, and specialized robots.

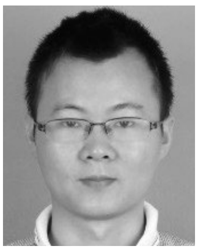

MIN CHENG was born in Jingzhou, China, in 1987. He received the B.S. and Ph.D. degrees in mechatronics from Zhejiang University, Hangzhou, China, in 2009 and 2015, respectively. He is currently a Lecturer with the State Key Laboratory of Mechanical Transmissions, College of Mechanical Engineering, Chongqing University, Chongqing, China. He is also a Researcher with the State Key Laboratory of Fluid Power and Mechatronic Systems, Zhejiang University. His research interests include electrohydraulic control systems of mobile machinery, energy saving and motion control of hydraulic systems, and mechatronic systems design.

BING XU was born in Anshan, China, in 1971. He received the Ph.D. degree in fluid power transmission and control from Zhejiang University, Hangzhou, China, in 2001. He is currently a Professor and a Ph.D. Tutor with the Institute of Mechatronic Control Engineering and also the Deputy Director with the State Key Laboratory of Fluid Power Transmission and Control, Zhejiang University. He has authored or coauthored more than 200 journal and conference papers, and authorized 49 patents. His research interests include fluid power components and systems, mechatronic systems design, energy saving, and motion control for mobile machinery. He is a Chair Professor of the Yangtze River Scholars Program and a Science and Technology Innovation Leader of the Ten Thousand Talent Program.

RUQI DING was born in Nanchang, China, in 1987. He received the Ph.D. degree in mechatronics from Zhejiang University, Hangzhou, China, in 2015. He is currently a Lecturer with the School of Mechatronic Engineering, East China Jiaotong University, Nanchang. His research interests include energy saving and motion control of electrohydraulic systems in mobile machinery, and mechatronic system design.

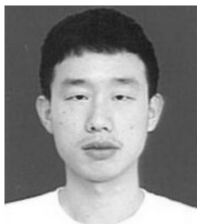

ZENAN HAN was born in Shaoxing, China, in 1996. He received the B.Eng. degree from the Zhejiang University of Technology, in 2018. He is currently pursuing the master's degree with the College of Mechanical Engineering, Chongqing University. His current research interests include fluid transmission and master-slave control.